ECCOMAS Congress 2016
VII European Congress on Computational Methods in Applied Sciences and Engineering
M. Papadrakakis, V. Papadopoulos, G. Stefanou, V. Plevris (eds.)
Crete Island, Greece, 5–10 June 2016

TOWARDS MULTIPHYSICS SIMULATION OF DEEP PENETRATION LASER WELDING USING SMOOTHED PARTICLE HYDRODYNAMICS

Haoyue Hu[1], Peter Eberhard[1], Florian Fetzer[2], and Peter Berger[2]

[1] Institute of Engineering and Computational Mechanics
University of Stuttgart
Pfaffenwaldring 9, 70569 Stuttgart, Germany
{haoyue.hu, peter.eberhard}@itm.uni-stuttgart.de

[2] Institut für Strahlwerkzeuge
University of Stuttgart
Pfaffenwaldring 43, 70569 Stuttgart, Germany
{florian.fetzer, peter.berger}@ifsw.uni-stuttgart.de

Keywords: Laser Welding, SPH, Phase Transition, Recoil Pressure, Ray Tracing, Co-Simulation.

Abstract. *Multiphysics simulations of deep penetration laser welding are performed with the meshless Lagrangian Smoothed Particle Hydrodynamics (SPH) method. Compared to mesh-based methods, SPH has advantages in handling phase transitions, free-surface melt flow, and fluid-structure interaction. Based on previous work on simulating conduction mode laser welding using SPH, the numerical model is extended to include further physical effects such as evaporation and exertion of recoil pressure on the melt due to evaporation. Particular emphasis is placed on modeling the energy input through the laser beam. A co-simulation approach is developed by coupling an SPH code with a ray tracer that tracks the propagation of the laser beam in the keyhole in order to achieve spatial distributions of energy transferred to the melt layer. A surface detection and reconstruction algorithm is implemented to exchange current surface data. Simulation results of spot welding and seam welding are shown using this co-simulation approach. The developed model serves as a basis to investigate the influence and sensitivity of process parameters on the weld and to better understand transient effects around the keyhole leading to weld imperfections.*

1 INTRODUCTION

Laser welding is widely applied in industry nowadays. It offers significant advantages over conventional welding techniques, such as a small heat affected zone resulting in low mechanical and thermal distortions in the workpiece, high heating and cooling rates, and the ability to join dissimilar materials. Depending on the absorbed power density from the laser beam, laser welding is classified in conduction mode and deep penetration welding. During conduction mode welding, evaporation plays no significant role and the energy is transferred to a more or less flat surface. In contrast, during deep penetration welding, a part of the material evaporates and a vapor-filled capillary surrounded by molten material is formed by the vapor pressure exerted on the melt, a so-called keyhole. Multiple reflections of the laser beam on the walls of the keyhole lead to a very high absorbed intensity by the molten material. As the keyhole follows the movements of the laser beam along the weld joint, the melt flows around the keyhole and solidifies, producing a deep and narrow weld seam. Deep penetration welding is a preferred welding technique, distinguished by high efficiency and fast welding speeds. However, the process easily becomes unstable and weld imperfections like spatters, pores, cracks, and humping, may then occur.

To simulate the process of deep penetration welding, the novel contribution of this paper is that we extend a developed SPH model for conduction mode welding [1, 2] to include evaporation and exertion of recoil pressure on the melt due to evaporated material. Concerning the laser-material interaction, knowledge about the spatial intensity distribution as energy input is essential. We propose a co-simulation approach with a ray tracer that tracks the propagation of the laser beam in the keyhole to obtain spatial intensity distributions. Further steps during the co-simulation are the transformation of the intensities to heat sources, and the surface detection and reconstruction to send an updated surface geometry to the ray tracer.

2 MODELING WITH SPH

The SPH method was developed by Gingold and Monaghan [3] and Lucy [4]. As a meshless Lagrangian method, it has been successfully applied to problems with large deformations, fluid flow with free surfaces, multiphase flow, etc. [5]. In SPH a continuum is represented by a set of particles acting as discretization points. Material properties and field variables like velocity and acceleration are associated to each particle such that the overall state of the system is characterized properly. The particles interact with each other within a smoothing length h of a kernel function W. The evaluation of field variables and their derivatives for a particle is approximated by sums over all neighboring particles. As a general discretization method, all systems that are described by partial differential equations can be simplified to a set of ordinary differential equations.

The modeling approach for laser welding using the SPH method is based on previous work of simulating the conduction mode laser welding process [1, 2]. Therefore, only a short summary is given in the following. The solid material is modeled with solid SPH particles extended to a thermomechanically coupled formulation. For the liquid melt flow, the standard formulation of weakly compressible SPH proposed by Monaghan [5] is used. Additionally, a temperature-dependent surface tension model for thermocapillary flow as shown in [6] is implemented. Heat transfer through conduction is modeled based on [7]. Temperature-dependent material properties are taken into account, as an example, different heat conductivities and heat capacities for the solid and liquid phases are included in the model. For both solid and liquid phases, the conservation laws of mass, momentum, and energy are discretized and used as basis for the

interaction between solid particles, fluid particles, and also for the fluid-structure interaction. The developed model is implemented into the software package Pasimodo [8, 9], which is used for the welding simulations.

2.1 Phase transitions

During deep penetration welding, the occurring phase transitions are melting, solidification, evaporation, and condensation. For phase transitions from solid to liquid or vice versa, the latent heat of fusion H_f has to be considered. If the absorbed amount of heat exceeds the latent heat of fusion, the melting has completed. The particle type is then dynamically changed from a solid to a fluid particle during the simulation. On the contrary, during solidification heat is released from the material. If the released amount of heat exceeds the latent heat of fusion, the solidification has completed and the particle type is then changed from a fluid to a solid particle.

Analogously, for phase transitions from liquid to vapor, the latent heat of evaporation H_v has to be taken into account. Currently, the vapor phase is not simulated, instead, the particles are deleted during the simulation after the evaporation has completed. Thus, condensation is neglected.

The specific enthalpy h is used to characterize the thermal energy stored in the system. At constant pressure, the increase in enthalpy is equal to the amount of heat added to the system. Therefore, a change in enthalpy may be converted to a change in temperature with the heat capacity as proportionality factor. The specific enthalpy over temperature is plotted in Fig. 1, in which constant heat capacities c_s and c_l are used for the solid and liquid phase, and the latent heat of fusion H_f and evaporation H_v are considered in a transition range between two phases.

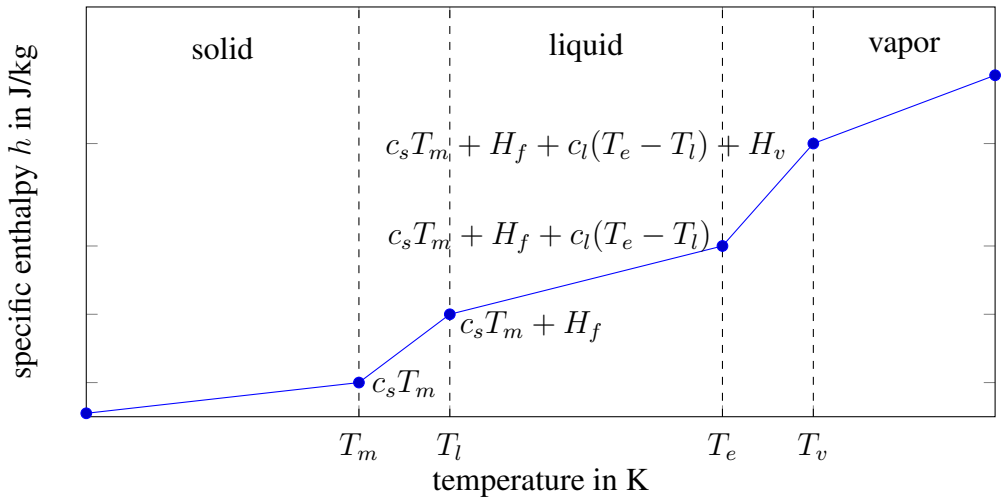

Figure 1: Specific enthalpy over temperature simplified as integrated values $\int c\,\mathrm{d}T$, i.e. the pressure changes are neglected here

2.2 Calculation of recoil pressure

Different models exist in literature for the calculation of recoil pressure acting on the surface of an evaporating material due to high-intensity laser irradiation [10, 11]. Here the physical model proposed in [12] is applied, since the predicted recoil pressures using this model are in reasonable agreement with experimental results.

The laser power absorbed by the material surface and spent in evaporation is

$$Q_s = Q_0\alpha(1-r) - Q_{\text{heat}} \ , \tag{1}$$

where Q_0 is the incident power of the laser beam, α the transmission coefficient in the laser-induced plasma plume, r the reflection coefficient at the material surface, and Q_{heat} the energy rate in W spent in heating and melting of the irradiated material. The recoil pressure is then evaluated as

$$p_s = \frac{Q_s}{AH_v}\sqrt{\frac{\pi k_B T_s}{2m_v}} \ , \tag{2}$$

in which A is the area of the laser spot at the surface, H_v is the latent heat of evaporation, k_B the Boltzmann constant, T_s the surface temperature, and m_v the mass of a vapor molecule. The Clausius-Clapeyron equation [13, 14]

$$\frac{p_a + p_s}{p_0} = \exp\left(\frac{m_v H_v}{k_B}\left(\frac{1}{T_v} - \frac{1}{T_s}\right)\right) \tag{3}$$

relates the pressure at the surface to the temperature at the surface. In Eq. (3) p_a is the environmental pressure, p_0 the atmospheric pressure, and T_v the evaporation temperature.

In [12] the value of Q_{heat} is obtained from empirical relations based on experimental results and Q_s is calculated for the whole surface. In the developed model, a local approach is applied instead and Q_s is approximated for each particle using its specific enthalpy

$$Q_s = \{h - [c_s T_m + H_f + c_l(T_e - T_l)]\}\frac{m}{\Delta t} \ , \tag{4}$$

where m is the mass of the particle, and Δt the time increment. To obtain both unknowns T_s and p_s, first the nonlinear equation

$$f(T_s) := \frac{p_a}{p_0} + \frac{Q_s}{p_0 A H_v}\sqrt{\frac{\pi k_B T_s}{2m_v}} - \exp\left(\frac{m_v H_v}{k_B}\left(\frac{1}{T_v} - \frac{1}{T_s}\right)\right) = 0 \tag{5}$$

is solved with the Newton-Raphson method, where the evaporation temperature is chosen as starting value $T_s^0 = T_v$. The iteration step

$$T_s^{n+1} = T_s^n - \frac{f(T_s)}{f'(T_s)} \tag{6}$$

with the derivative

$$f'(T_s) = \frac{\mathrm{d}f}{\mathrm{d}T_s} = \frac{Q_s}{2p_0 A H_v}\sqrt{\frac{\pi k_B}{2m_v T_s}} - \frac{m_v H_v}{k_B T_s^2}\exp\left(\frac{m_v H_v}{k_B}\left(\frac{1}{T_v} - \frac{1}{T_s}\right)\right) \tag{7}$$

is repeated until a relative or absolute convergence criterion is fulfilled, or if the maximum number of iterations is reached. Afterwards p_s is evaluated using Eq. (2) and the recoil pressure is added to all surrounding particles.

3 RAY TRACING ALGORITHM

A ray tracing algorithm introduced in [15] is applied to calculate the local absorbed intensity from the laser beam on a discretized surface. The idea is to use geometrical optics to track the propagation of independent light rays. The geometry of the surface is meshed with triangles and specified in STL format. During the calculation, a large number of rays are generated randomly based on a Monte Carlo method. The overall distribution of the rays corresponds to the intensity profile of the laser beam. When a ray hits a triangle, the local absorbed intensity is evaluated from the absorbed power of the ray divided by the area of that triangle. The absorption is calculated using the Fresnel equations [16]. Then the reflected ray is traced and the calculation of the local absorbed intensity is repeated. After multiple reflections are performed, the total absorbed intensity at each triangle is obtained from the sum of each absorbed intensity from individual rays at the triangle. If no intersection between a ray and the triangles is detected, the ray is deleted during the simulation.

The existing algorithm from [15] is extended to include further physical effects. Temperature-dependent optical material parameters are specified in a data table, and the values are interpolated in between. Furthermore, diffuse reflection according to Lambert's emission law may be chosen in addition to Fresnel absorption.

4 CO-SIMULATION APPROACH

To model the laser-material interaction, a co-simulation approach is developed with a server-client architecture, where Pasimodo [8, 9] acts as the server, and the ray tracer as a client. The data exchange is carried out via a TCP/IP network connection.

The procedure of the co-simulation is shown in Fig. 2. The initial surface as input for the ray tracer is taken as a circular plane. The calculated absorbed intensities for each triangle are transferred to Pasimodo as initial energy input through the laser beam. In Pasimodo heat source particles are added at the center of gravity positions of each triangle. To reduce the computational effort, only triangles with an absorbed intensity above a threshold value set as 100 W/m^2 are considered. In Pasimodo the welding simulation using SPH is performed with these dynamically added heat sources. After a user-defined time interval of Δt, the updated geometry of the free-surface melt flow and the temperature of the surface particles are sent to the ray tracer. The co-simulation loop is repeatedly executed until the welding simulation has finished. The additional steps performed during the co-simulation are explained in the following.

4.1 Transformation of intensities to heat sources

For the SPH simulation in Pasimodo, the absorbed intensities I_s are transformed to heat source particles at the center of gravity positions of each triangle. The radius of the heat source particle is set to

$$r_s = \sqrt{\frac{A_s}{\pi}} = \sqrt{\frac{\frac{1}{2}\|\mathbf{a} \times \mathbf{b}\|}{\pi}} \,, \tag{8}$$

where A_s is the area of the triangle which may be obtained by half the norm of the cross product of two edge vectors $\mathbf{a}$, $\mathbf{b}$ originating from one vertex, see Fig. 3. All neighboring particles with a distance less than $2r_s$ interact with the heat source particle. To ensure that the total power added to all neighboring SPH particles is equal to the absorbed power from the laser beam at the triangle, a correction factor is determined similarly to [17]. The correction factor is evaluated

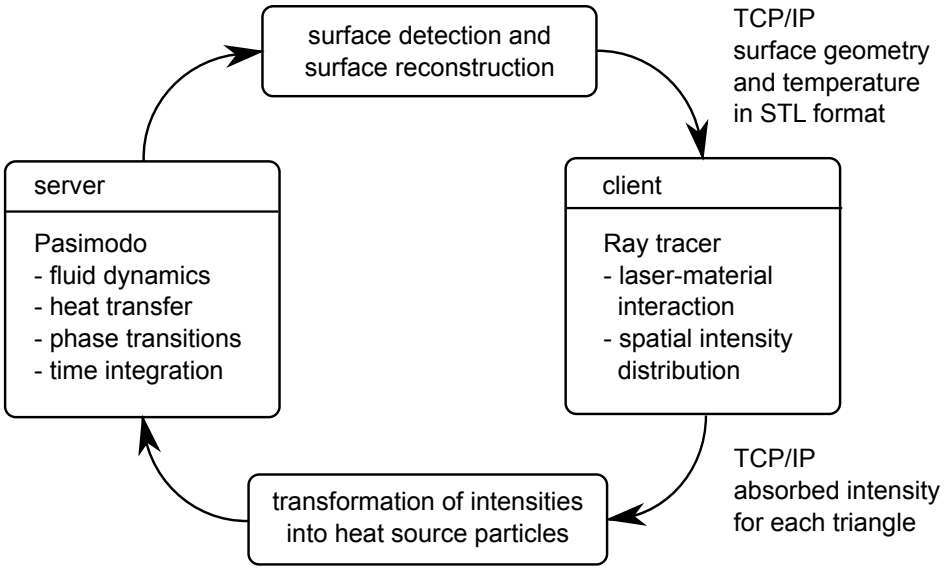

Figure 2: Co-simulation loop

as the total volume of the neighboring particles,

$$\zeta_s = \sum_j \frac{m_j}{\rho_j} = \sum_j V_j \,, \tag{9}$$

where m_j is the mass, ρ_j the density, and V_j the volume of particle j. Afterwards, a source term

$$\frac{1}{\rho_j} \frac{I_s A_s}{\zeta_s} \tag{10}$$

in the unit W/kg is added to the right hand side of the energy equation for each SPH particle within a distance of $2r_s$.

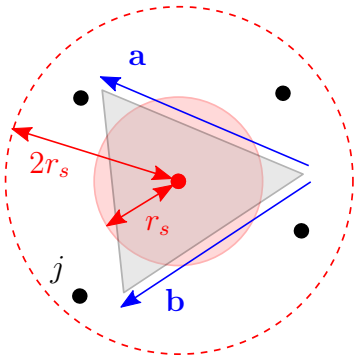

Figure 3: Transformation of a triangle into a heat source particle with radius r_s interacting with its neighbor particles j within a distance of $2r_s$

4.2 Surface detection algorithm

The applied algorithm for the detection of surface particles in the vicinity of the laser beam is adopted from [18] which combines the ideas given in [19] and [20]. For each particle i the normal vector of the surface is approximated by a so-called cover vector

$$\mathbf{b}_i = \sum_j \frac{\mathbf{x}_i - \mathbf{x}_j}{\|\mathbf{x}_i - \mathbf{x}_j\|} , \tag{11}$$

which is evaluated based on the distance to its neighbor particles j. Around the cover vector, a scan cone is defined with an apex angle of θ, as shown in Fig. 4. In a second step, it is checked if at least another neighbor particle is located in the scan cone created by $\mathbf{b}_i$. An interior particle has to fulfill the condition

$$\arccos\left(\frac{\mathbf{x}_j - \mathbf{x}_i}{\|\mathbf{x}_j - \mathbf{x}_i\|} \cdot \frac{\mathbf{b}_i}{\|\mathbf{b}_i\|}\right) \leq \frac{\theta}{2} \tag{12}$$

for at least one neighbor particle j, otherwise the considered particle i is regarded as surface particle. In Fig. 4 the dashed circle has the radius of the smoothing length h of particle i. All neighboring particles located in the influence range contribute to the cover vector, and Eq. (12) is checked for each of them. In Fig. 4(a) particle i is detected as a surface particle, since there are no other particles located in the scan cone created by $\mathbf{b}_i$. In Fig. 4(b), however, there is a neighbor particle located in the scan cone, for which Eq. (12) is satisfied. Therefore, particle i is identified as an interior particle in this case.

This method is rather simple and fast, but it is not always accurate. Especially for randomly distributed particles, interior particles may be detected as surface particles and vice versa. Another drawback is the detection of different surface particles depending on different apex angles set for the scan cone. Here the angle θ is set to 60° in accordance with [18].

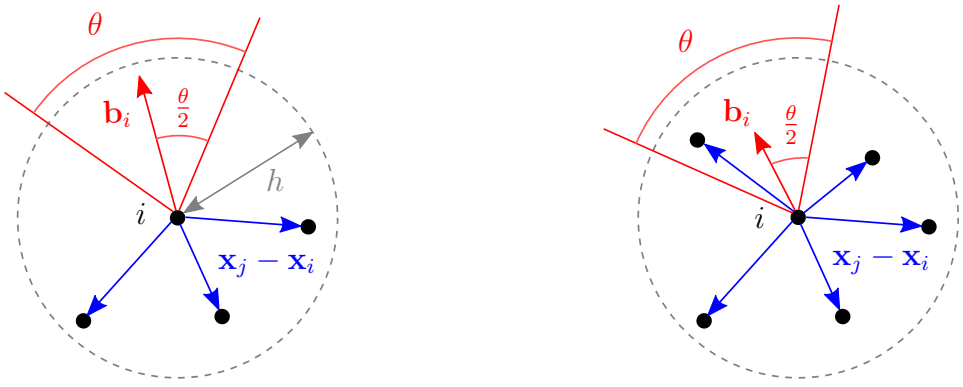

(a) Particle i is a surface particle, since no other particles are located in the scan cone

(b) Particle i is an interior particle, since a neighbor particle is detected in the scan cone

Figure 4: 2D example of a small set of SPH particles to illustrate the surface detection algorithm

4.3 Surface reconstruction algorithm

After all relevant surface particles are detected, the surface is reconstructed and a surface mesh consisting of triangles is created for the next simulation loop with the ray tracer. The

surface mesh is obtained with a Delaunay triangulation [21], in which the surface particles act as vertices of the triangles. Delaunay triangulations tend to avoid badly shaped triangles by maximizing the minimum angle of all triangles. There are several algorithms implementing the Delaunay triangulation method with $O(n \log n)$.

The applied algorithm is from [22, 23] which is based on randomized incremental construction. Currently, a 2D triangulation is performed based on the x- and y-coordinates of detected surface particles. Afterwards, the vertices of the triangles are shifted in z-direction. This approach is inadequate for keyhole geometries with undercuts, but works well for convex geometries.

After the triangulation function call which delivers an index list of all triangles, the surface geometry and temperature data are sent to the ray tracer in binary STL format. The surface temperature of each triangle is approximated as mean value of the temperatures at its vertices.

5 EXAMPLES

To evaluate the co-simulation approach, two characteristic welding examples are chosen. The first example is spot welding of iron, and the second example is seam welding of aluminum. For both simulation examples the co-simulation loop is repeated every 0.1 ms.

5.1 Spot welding of iron

This example shows the formation of a keyhole during spot welding of iron. The applied laser beam has a power of 3 kW and a spot diameter of 0.3 mm. The surface geometry of the melt pool which is sent from Pasimodo to the ray tracer is shown for several time instants in Figure 5. For the given set of process parameters, the aspect ratio of depth to spot radius is approximately one at 0.5 ms, which marks the threshold from conduction mode to deep penetration welding. The aspect ratio increases to two at 1.5 ms.

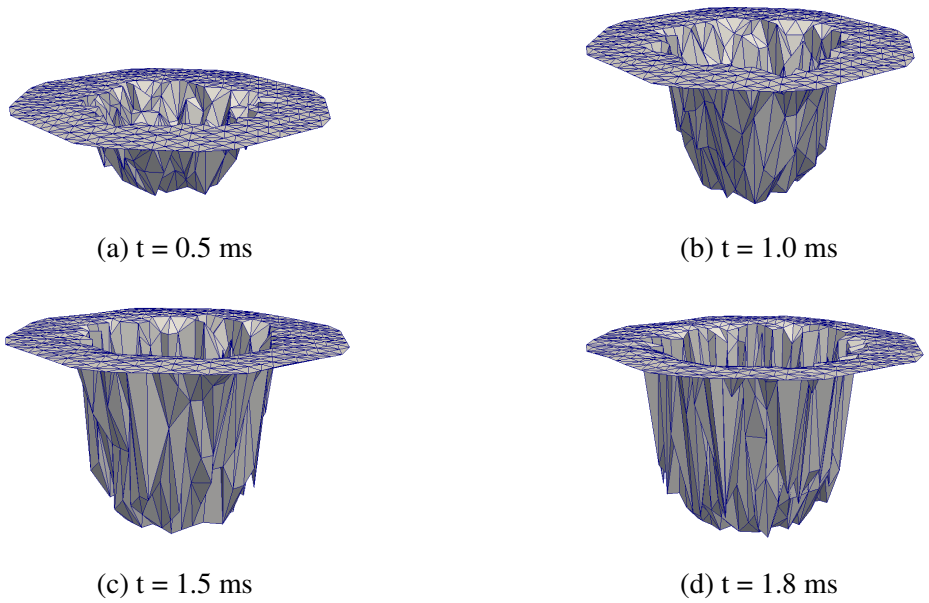

(a) t = 0.5 ms (b) t = 1.0 ms

(c) t = 1.5 ms (d) t = 1.8 ms

Figure 5: STL surface geometries sent from Pasimodo to the ray tracer which illustrate the formation of a keyhole during spot welding of iron

The temperature distribution around the keyhole at $t = 2\,\text{ms}$ is shown in Fig. 6. The evaporated particles are deleted during the simulation and thus, are not displayed. Nearly all surface particles around the keyhole have reached the evaporation temperature, but the absorbed amount of heat is still less than the latent heat of evaporation. The particles at the tip of the keyhole have a lower temperature, which indicates that the particle layer above have evaporated almost instantaneously shortly before the depicted instant of time. Therefore, both the evaporated particles and the laser beam did not have enough time to heat the current surface layer at the tip of the keyhole up to evaporation temperature.

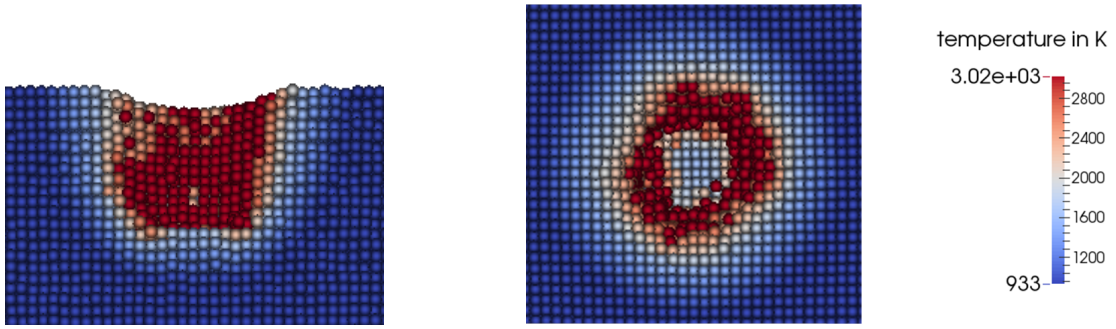

(a) view at mid cross section (b) view at top surface

Figure 6: Temperature distribution in the vicinity of the keyhole at $t = 2\,\text{ms}$

5.2 Seam welding of aluminum

As another example, seam welding of aluminum is simulated with a constant welding speed of 25 m/min. The laser power is set to 4.5 kW and the laser spot diameter is 0.6 mm. In Fig. 7 the SPH particles are colored based on the number of phase transitions. The particles in grey form the liquid weld pool, the particles in red were melted and solidified to form the resulting weld, and the particles in blue remained solid during the welding process. Again, we can analyze the aspect ratio of depth to spot radius, which is slightly larger than one, indicating that the threshold for deep penetration welding is reached. This corresponds well with the fact that some particles at the center have evaporated, but the amount of evaporated material is not large enough to form a considerable keyhole that results in a deep weld seam.

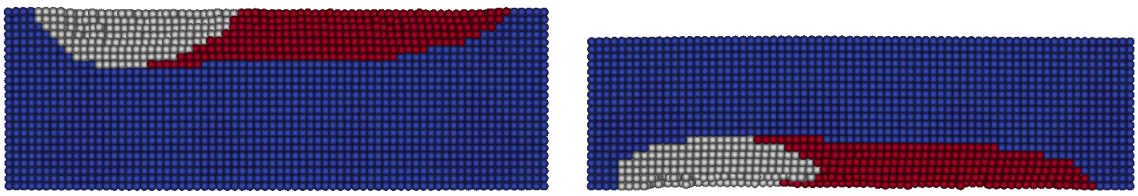

(a) view at mid cross section (b) view at half of the top surface

Figure 7: Seam welding of aluminum with weld pool colored in grey and solidified weld colored in red

6 CONCLUSIONS

The process of laser welding is simulated using the SPH method, where both the solid and liquid phase are modeled including significant physical effects such as surface tension, heat conduction, and thermal expansion. The phase transitions melting, solidification, and evaporation are taken into account together with the absorption or release of the latent heat of fusion and evaporation. The evaporated material is currently not modeled, but the recoil pressure that affects the melt is implemented based on a physical model in [12].

A co-simulation approach is developed by coupling an SPH code with a ray tracer to capture the laser-material interaction for complicated surface geometries. The data exchange is based on a TCP/IP protocol. Preliminary steps to the data exchange are the transformation of intensities into heat source particles interacting with other SPH particles at the surface of the melt, the surface detection, and the surface reconstruction. Suitable algorithms are chosen from literature and implemented. The obtained results are promising, but there are still some drawbacks and limitations in the implemented versions.

For future work, more complex algorithms for surface detection and reconstruction shall be implemented to better characterize the keyhole during laser welding. The goal is then to investigate instabilities that arise during the process, such as pore formation, spatter, and humping. This will be done numerically and also experimentally.

ACKNOWLEDGEMENT

The research leading to the presented results has received funding from the German Research Foundation (DFG) under the project EB 195/13-1 and GR 3172/18-1 “Modeling of the capillary in laser beam penetration welding with the Smoothed Particle Hydrodynamics Method”. This support is highly appreciated.

REFERENCES

[1] H. Hu, P. Eberhard, Two-Phase Modeling of Conduction Mode Laser Welding Using Smoothed Particle Hydrodynamics. In Proceedings of the IV International Conference on Particle-based Methods - Fundamentals and Applications (PARTICLES 2015), Barcelona, Spain, September 28-30, 2015.

[2] H. Hu, P. Eberhard, Thermomechanically Coupled Conduction Mode Laser Welding Simulations Using Smoothed Particle Hydrodynamics. Computational Particle Mechanics, 2016 (submitted for publication).

[3] R.A. Gingold, J.J. Monaghan, Smoothed Particle Hydrodynamics: Theory and Application to Non-Spherical Stars. Monthly Notices of the Royal Astronomic Society, Vol. 181, pp. 375–389, 1977.

[4] L.B. Lucy, A Numerical Approach to the Testing of the Fission Hypothesis. The Astronomical Journal, Vol. 82, No. 12, pp. 1013–1024, 1977.

[5] J.J. Monaghan, Smoothed Particle Hydrodynamics and Its Diverse Applications. Annual Review of Fluid Mechanics, Vol. 44, pp. 323–346, 2012.

[6] M. Tong, D.J. Browne, An Incompressible Multi-Phase Smoothed Particle Hydrodynamics (SPH) Method for Modelling Thermocapillary Flow. International Journal of Heat and Mass Transfer, Vol. 73, pp. 284–292, 2014.

[7] P.W. Cleary, J.J. Monaghan, Conduction Modelling Using Smoothed Particle Hydrodynamics. Journal of Computational Physics, Vol. 148, pp. 227–264, 1999.

[8] F. Fleissner, Parallel Object Oriented Simulation with Lagrangian Particle Methods. Schriften aus dem Institut für Technische und Numerische Mechanik, Vol. 16. Aachen: Shaker Verlag, 2010.

[9] Pasimodo, http://www.itm.uni-stuttgart.de/research/pasimodo. Accessed March 14, 2016.

[10] S.I. Anisimov, Vaporization of Metal Absorbing Radiation. Soviet Physics, Journal of Experimental and Theoretical Physics, Vol. 27, No. 1, pp. 182–183, 1968.

[11] V. Semak, A. Matsunawa, The Role of Recoil Pressure in Energy Balance During Laser Materials Processing. Journal of Physics D: Applied Physics, Vol. 30, pp. 2541–2552, 1997.

[12] X. Chen, H.-X. Wang, A Calculation Model for the Evaporation Recoil Pressure in Laser Material Processing. Journal of Physics D: Applied Physics, Vol. 34, pp. 2637–2642, 2001.

[13] R. Clausius, Über die bewegende Kraft der Wärme und die Gesetze, welche sich daraus für die Wärmelehre selbst ableiten lassen (in German). Annalen der Physik, Vol. 155, pp. 500–524, 1850.

[14] M.C. Clapeyron, Mémoire sur la Puissance Motrice de la Chaleur (in French). Journal de l'École Polytechnique, Vol. 23, pp. 153–190, 1834.

[15] A. Michalowski, Untersuchungen zur Mikrobearbeitung von Stahl mit ultrakurzen Laserpulsen (in German). Doctoral thesis, Institut für Strahlwerkzeuge (IFSW), University of Stuttgart. Munich: Herbert Utz Verlag, 2014.

[16] E. Hecht, Optics, 4th Edition. San Francisco: Addison-Wesley, 2002.

[17] J.J. Monaghan, H. Huppert, M. Worster, Solidification Using Smoothed Particle Hydrodynamics. Journal of Computational Physics, Vol. 205, pp. 684–705, 2005.

[18] A. Barecasco, H. Terissa, C.F. Naa, Simple Free-Surface Detection in Two and Three-Dimensional SPH Solver. Selected Paper from the International Symposium on Computational Science 2013, Kanazawa, Japan, 2013.

[19] H. Aamer, G.A. Dilts, Three-Dimensional Boundary Detection for Particle Methods. Journal of Computational Physics, Vol. 226, pp. 1710–1730, 2007.

[20] S. Marrone, Fast Free-Surface Detection and Level-Set Function Definition on SPH Solvers. Journal of Computational Physics, Vol. 229, pp. 3652–3663, 2010.

[21] B. Delaunay, Sur la Sphère Vide (in French). Bulletin de l'Académie des Sciences de l'URSS, Classe des Sciences Mathématiques et Naturelles, Vol. 6, pp. 793–800, 1934.

[22] K.L. Clarkson, K. Mehlhorn, R. Seidel, Four Results on Randomized Incremental Constructions. Computational Geometry: Theory and Applications, Vol. 3, pp. 185–212, 1993.

[23] K.L. Clarkson, Safe and Effective Determinant Evaluation. In Proceedings of 31st IEEE Symposium on Foundations of Computer Science, 387–395, Pittsburgh, USA, 1992.